Available online at www.sciencedirect.com
ScienceDirect
Earth and Planetary Science Letters 256 (2007) 169–181
EPSL
www.elsevier.com/locate/epsl

Compactional deformation bands in Wingate Sandstone; additional evidence of an impact origin for Upheaval Dome, Utah

Chris H. Okubo [a,*], Richard A. Schultz [b]

[a] *Lunar and Planetary Laboratory, University of Arizona, Tucson, AZ 85721, United States*
[b] *Geomechanics-Rock Fracture Group, Department of Geological Sciences and Engineering/172, University of Nevada, Reno, NV 89557-0138, United States*

Received 28 April 2006; received in revised form 8 January 2007; accepted 21 January 2007
Available online 27 January 2007
Editor: G.D. Price

Abstract

Field and microstructural observations from Upheaval Dome, in Canyonlands National Park, Utah, show that inelastic strain of the Wingate Sandstone is localized along compactional deformation bands. These bands are tabular discontinuities (<0.5 cm thick) that accommodate inelastic shear and compaction of inter-granular volume. Measurements of porosity and grain size from non-deformed samples are used to define a set of capped strength envelopes for the Wingate Sandstone. These strength envelopes reveal that compactional deformation bands require at least *ca.* 0.7 GPa (and potentially more than 2.3 GPa) of effective mean stress in order to nucleate within this sandstone. We find that the most plausible geologic process capable of generating these required magnitudes of mean stress is a meteoritic impact. Therefore the compactional deformation bands observed within the Wingate Sandstone are additional evidence of an impact event at Upheaval Dome and support a post-Wingate (post-Early Jurassic) age for this impact.

Keywords: Upheaval Dome; deformation band; Wingate Sandstone; impact crater; Canyonlands National Park

1. Introduction

Upheaval Dome is a prominent quasi-circular structure located within the Island in the Sky district of Canyonlands National Park, Utah ([1,2]; Fig. 1). This *ca.* 5.5-km wide structure exposes Permian to Jurassic-aged sedimentary rocks ([1,3]; Fig. 2). The oldest and most pervasively deformed rocks exposed at Upheaval Dome occur within a central dome-shaped mound, which is encircled by outward-dipping monoclines of younger strata.

Rocks exposed at Upheaval Dome are Permian to Jurassic in age (Fig. 2). The oldest rocks consist of White Rim Sandstone, which consists of coastal eolian sediment and is present in Upheaval Dome only as cataclastic dikes intruded into the overlying strata. The Moenkopi Formation stratigraphically overlies the White Rim Sandstone and consists of fluvial to shallow marine sediment. The central uplift of Upheaval Dome consists of rocks of the Moenkopi Formation and cataclastic dikes of White Rim Sandstone. Overlying the Moenkopi Formation is the Chinle Formation, which consists of fluvial sediment. The Wingate Sandstone

* Corresponding author. Tel.: +1 520 626 1458; fax: +1 520 626 8998.
E-mail address: chriso@lpl.arizona.edu (C.H. Okubo).

0012-821X/$ - see front matter © 2007 Elsevier B.V. All rights reserved.
doi:10.1016/j.epsl.2007.01.024

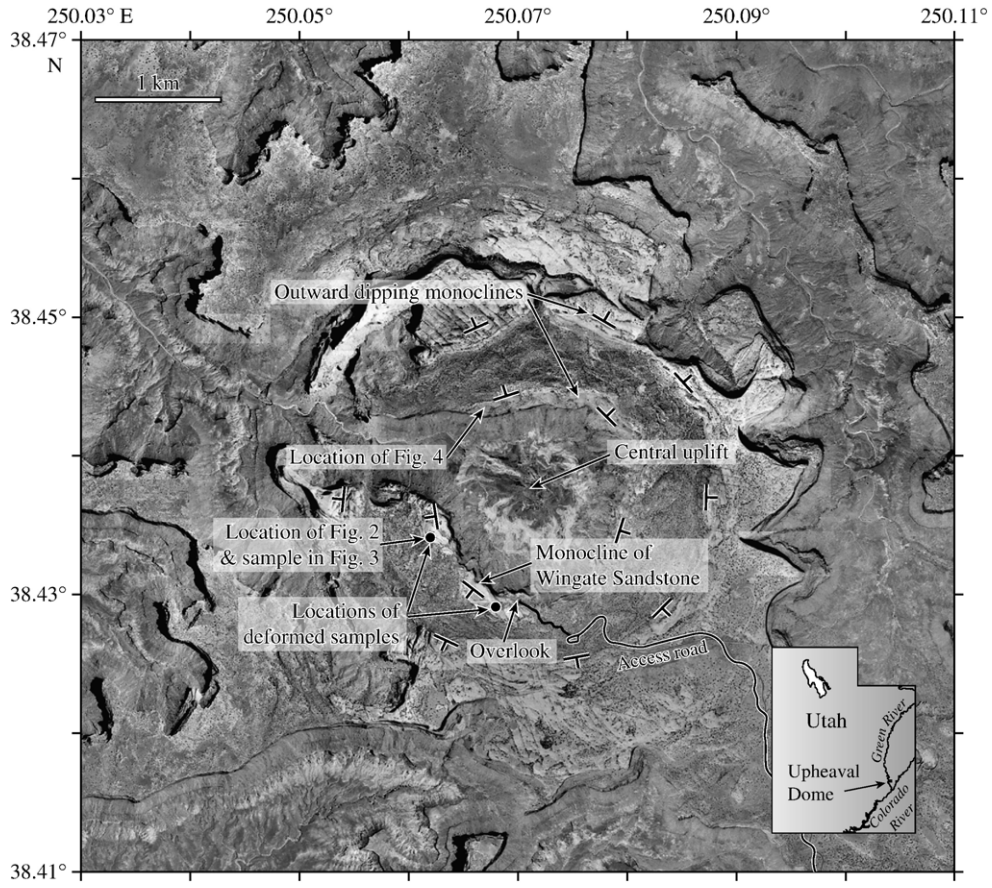

Fig. 1. Orthophotograph of Upheaval Dome showing the central uplift surrounded by concentric, outward-dipping monoclines of younger stratigraphic units. The Wingate Sandstone outcrops along the inner-most monocline. Dip directions are based on Jackson et al. [13], and the orthophotograph from the U.S. Geological Survey [2]. Illumination is from the bottom of the image.

overlies the Chinle Formation and is composed of wet erg deposits. The Wingate Sandstone forms prominent 100-m-high cliffs that encircle the central uplift. Overlying the Wingate Sandstone are the fluvial deposits of the Kayenta Formation and the eolian Navajo Sandstone.

Various origins for Upheaval Dome have been proposed. Two commonly cited origins are meteoritic impact [3–9] and salt diapirism from the subjacent Pennsylvanian-aged Paradox Formation [10–13]. Upheaval Dome has also been interpreted to be the result of igneous intrusion [10,11], explosive volcanism [14] or tectonically driven fluid overpressure [15], however these three latter mechanisms are not supported by recent literature. Recent seismic imaging of a flat-topped subjacent Paradox Formation [7] does not support salt diapirism and is instead consistent with meteoritic impact. Detailed mapping of Upheaval Dome [3,6,8,9] also reveals discrete structural elements that are consistent with impact craters [16]. Meteoritic impact interpretations for Upheaval Dome suggest that the original crater diameter was *ca.* 5–9 km [3,4,9] prior to erosion.

Recent microstructural analyses have also provided compelling evidence in support of a meteoritic impact origin for Upheaval Dome. Field reconnaissance reveals the presence of shatter cones in the Moenkopi Formation [6]. Baratoux and Melosh [17] show that shatter cones generally form at magnitudes of mean stress, P, between 3 GPa and 6 GPa. Additionally, the cataclastic dikes of White Rim Sandstone require magnitudes of P in excess of 0.25 GPa in order to form [8]. Cataclastic dikes of Wingate Sandstone are also observed within the overlying Kayenta Formation and underlying Chinle Formation [6,8,9,18]. Furthermore, planar-deformed quartz grains occur within the cataclastic dikes of White Rim Sandstone [6,8]. TEM and SEM analyses of deformed quartz grains from these cataclastic dikes reveal microcracks, isolated

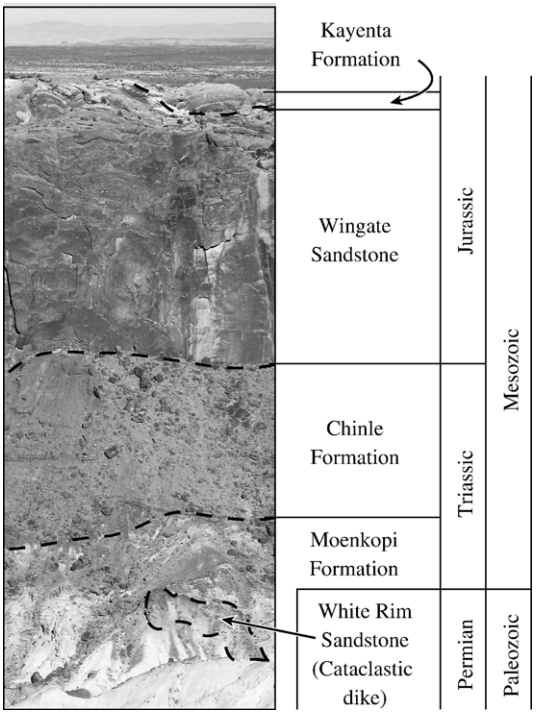

Fig. 2. Cross sectional view of stratigraphic units in Upheaval Dome as exposed in the inner-most cliffs surrounding the central uplift (see Fig. 1 for location; view is toward the North). The cliff-forming Wingate Sandstone is approximately 100 m thick and is overlain by the Kayenta Sandstone.

dislocations, dislocation arrays, dislocation loops and dislocation tangles [8]. Amorphous planar deformation features are not observed [8]. The style of deformation observed within these quartz grains indicates that the causative magnitude of P was less than the dynamic elastic limit of quartz (3 GPa to 15 GPa; [8]). The style of this planar deformation of quartz is consistent with Kieffer's [19] 'b1' classification, indicating magnitudes of P of up to 5.5 GPa [4,6]. These studies unanimously conclude that the attendant magnitudes of causative mean stress (*ca.* 0.25 GPa to 3 GPa) point to a meteoritic impact origin for Upheaval Dome.

The age of Upheaval Dome is poorly constrained. Proposed synsedimentary liquefaction structures within the Carmel Formation and Slickrock Member of the Entrada Sandstone (not exposed at Upheaval Dome) have been attributed to impact-related ground shaking during the Middle Jurassic [20]. Numerical modeling based on observed macro- and microscructural deformation supports a Late Cretaceous age for the impact event [9]. Impact crater depth to diameter scaling relations applied to Upheaval Dome (accounting for erosion since formation) places the impact event within the Late Cretaceous to Early Tertiary [4].

Evidence for a meteoritic impact at Upheaval Dome has so far been reported in Permian and Triassic-aged rocks (i.e., the White Rim Sandstone, Moenkopi Formation). The large magnitudes of impact-induced P are expected to extend into the overlying strata that were present at the time of the impact event [9]. The Jurassic-aged Wingate Sandstone predates proposed impact ages for Upheaval Dome and thus may contain additional evidence of this impact event.

In this paper, we show that field and microstructural observations of localized inelastic deformation (cataclastic deformation bands) within the Wingate Sandstone (Fig. 3) reveal additional evidence for the large magnitudes of P that support an impact origin for Upheaval Dome. This paper details our general methodology, and technical background, then presents preliminary results and directions for future work.

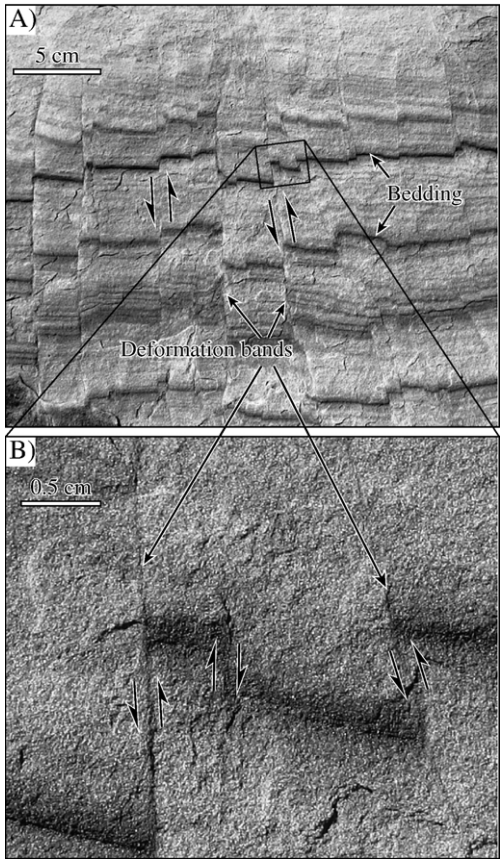

Fig. 3. (A) Inelastic deformation localized along fractures within the Wingate Sandstone at Upheaval Dome. (B) Shear displacements of light and dark-toned sedimentary bedding indicate that these fractures are deformation bands. These deformation bands erode out of the host rock with both positive and negative relief. This outcrop is horizontal and planar. See Fig. 1 for location.

2. Technical background

We use field and microstructural analyses to calculate the range of stress magnitudes that are required to cause observed styles of localized inelastic deformation of the Wingate Sandstone at Upheaval Dome. These stress magnitudes are then compared with previous findings of GPa-scale mean stresses within the central uplift. Our analyses are based on recent advances in understanding the mechanical processes that control elastic and inelastic deformation of granular rocks and soils. Examples of granular geomaterials (i.e., rocks and soils) include poorly to well-indurated sandstone (e.g., Wingate Sandstone), volcanic pyroclastic deposits, and limestone (e.g., [21–23]).

In this section, we show how principles of granular rock mechanics yield insight into the magnitudes of stress that are required to induce inelastic deformation within granular geomaterials such as the Wingate Sandstone. We then apply these principles to the observed deformation at Upheaval Dome.

2.1. Strength envelope for granular geomaterials

The strength of granular rocks and soils is commonly quantified in terms of the differential stress, Q, and effective mean stress, P, invariants;

$$Q = \sigma_1 - \sigma_3 \tag{1}$$

$$P = \frac{\sigma_1 - \sigma_2 - \sigma_3}{3} - p_i \tag{2}$$

where σ_1 and σ_3 are the largest and smallest compressive principal stresses respectively and P_i is pore fluid pressure (e.g., [21,24]). A strength envelope in Q–P space is commonly used to define the critical stress states at which strain in granular rocks and soils transitions from elastic to inelastic (e.g., [22,24–26]). This approach to quantifying the strength of granular geomaterials is analogous to the frictional (e.g., Coulomb) strength envelope in shear stress–normal stress space for crystalline rocks.

Two widely used strength envelopes for rocks are Coulomb (e.g., [27,28]) and Hoek–Brown [29]. The Coulomb strength envelope is appropriate for soils at low magnitudes of P and for crystalline rock, while Hoek–Brown is used to describe the strength of fractured rock masses. These strength envelopes are measures of the amount of energy required: (1) to move fracture surface asperities past each other by dilation of the slipping fracture surfaces, and (2) to detach fracture surfaces held together by cohesion. These strength envelopes are therefore strictly appropriate for describing the onset of inelastic strain (fracture displacement) through dilation along discontinuities. Dilation-dominant strength envelopes are suitable for geomaterials that have a dilational strength that is smaller than the attendant compactional strength; that is, the materials fail in effective tension before failing in compression. Dilation-dominant strength envelopes are therefore poorly suited to describe the behavior of geomaterials that can undergo inelastic *compaction* at stress levels that are *less than* the magnitudes of stress that are required for dilational failure; essentially compaction-dominant strength behavior.

A compaction-dominant strength behavior is exhibited by granular rocks and soils under large magnitudes of P [25] (Fig. 4). During the compactional failure of granular geomaterials, the application of shear stress (Q) drives constituent grains into a more efficient packing geometry through particle rotations and translations in a process termed ‘shear-enhanced compaction’ [22]. Grain crushing can also occur as an additional mode of compactional yielding [22,24,30] and enhances packing efficiency by generating smaller particles that can fit into the spaces between larger grains. These processes of compaction result in an inelastic reduction (closure) of inter-granular space.

Thus two distinct modes of inelastic strain, dilation and compaction, are observed in granular rocks and soils. The specific mode of failure (dilation or compaction) corresponds to the relative magnitude of P at the onset of inelastic strain. At small magnitudes of P, inelastic strain occurs by dilation of inter-granular space along a fracture surface. At large magnitudes of P, inelastic strain occurs by compaction of inter-granular

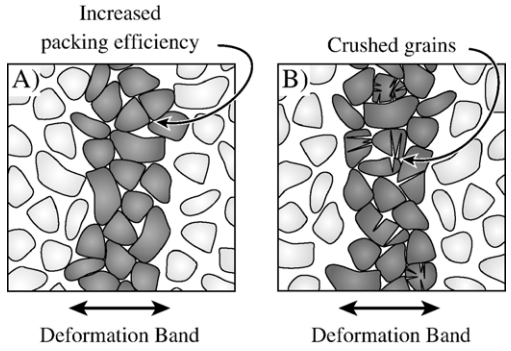

Fig. 4. Evidence of mechanical compaction along deformation bands. (A) Decreased inter-granular void space (i.e., enhanced packing efficiency) relative to the surrounding host rock. (B) Grain crushing through the growth of opening mode fractures at grain-to-grain contacts.

space and potentially by grain crushing. Therefore a complete strength envelope for granular rocks and soils must be able to describe the onset of inelastic *dilation* at small magnitudes of P and the transition to inelastic *compaction* at large magnitudes of P.

In order to describe the transition from inelastic dilation to inelastic compaction with increasing magnitudes of P, strength envelopes for granular geomaterials have been formulated that place a 'cap' on the maximum magnitudes of P (for a given Q) for which elastic strain persists (Fig. 5). This 'cap' delineates the transition from elastic to inelastic compactional strain and transitions into the dilational part of the overall 'capped strength envelope' at smaller magnitudes of P. The transition from inelastic compaction to dilation occurs at the apex of the capped strength envelope, where Q is maximum and inelastic strain is isochoric (simple shear). Elastic strain persists for (Q, P) stress states circumscribed by this capped strength envelope, and inelastic strain occurs for stress states that fall outside of this envelope.

Capped strength behavior in granular geomaterials has been extensively observed and quantified through laboratory testing (e.g., [22,24]). Constitutive models of capped strength envelopes have also been developed for soils [27,31] and granular rocks (e.g., [32–34]).

The capped strength envelope for granular rocks and soils is the foundation for the analyses presented in this paper. This envelope relates specific ranges of a causative P to a specific style of observed inelastic strain (dilation or compaction; Fig. 5). Accordingly, a capped strength envelope for Wingate Sandstone is used in this paper to determine the ranges of P that were required

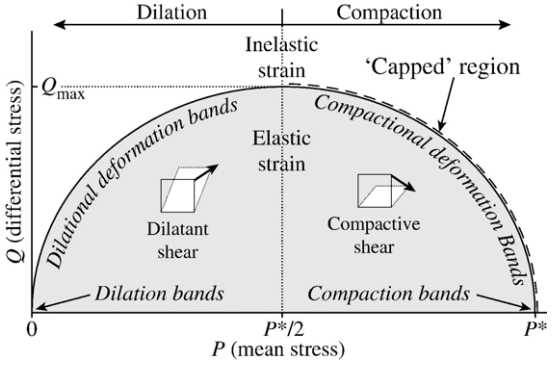

Fig. 5. The general features of a capped strength envelope for granular geomaterials in mean stress (P) and differential stress (Q) space. The capped region of the envelope describes the stress states for the onset of inelastic compaction and transitions to the inelastic dilation side of the envelope at Q_{max}. P^* is the grain crushing pressure (see Eq. (4)). This diagram shows how the type of band observed in the field can be related back to a causative Q,P stress state.

to cause the style of deformation that is observed at Upheaval Dome. The style of deformation is established through direct observations. The required magnitudes of P are then used as admissibility criteria in our assessment of potential causative geologic processes for this deformation. Candidate geologic processes that are found to be capable of causing the observed deformation of the Wingate Sandstone are subsequently discussed in the broader context of Upheaval Dome.

2.2. Manifestations of inelastic strain

In Q–P space, the capped strength envelope marks the stress states at which elastic deformation transitions to inelastic strain. This inelastic strain is manifest through a variety of geologic structures. In this section, we summarize the types of discontinuities that form in response to the onset of inelastic strain in granular geomaterials. This discussion establishes the diagnostic styles of inelastic strain that might be expected to occur within the Wingate Sandstone at Upheaval Dome.

Dilational inelastic strain occurs at small to moderate magnitudes of P along the capped strength envelope (Fig. 5). Where P is small but non-trivial and Q is zero, tabular discontinuities called 'dilation bands' [35] form through localized increases in inter-granular volume (dilation) and zero shear strain. At increasing values of Q and P, inelastic strain occurs through increasing magnitudes of shear and decreasing magnitudes of dilation respectively. This process of 'shear-enhanced dilation' [22,24] drives the growth of tabular discontinuities termed in this paper as 'dilational deformation bands'.

The capped strength envelope peaks at a maximum Q value, Q_{max}, which delineates the 'dilational side' of the envelope at smaller magnitudes of P from the 'compactional side' (i.e., the cap) at larger magnitudes of P (Fig. 5). At Q_{max}, inelastic strain occurs through localized simple shear and is manifest through the formation of 'isochoric deformation bands', or deformation bands with zero change in inter-granular volume (e.g., [26]).

Compactional inelastic strain occurs at moderate to large magnitudes of P along the capped strength envelope (Fig. 5). Within this range of P, and where Q is less than Q_{max} and non-trivial, inelastic strain occurs through shear and inter-granular volume loss (compaction). This process of 'shear-enhanced compaction' [22,24] can localize inelastic strain along tabular discontinuities termed here as 'compactional deformation bands'. At the maximum value of P, with zero Q, inelastic strain occurs through localized compaction without shear along 'compaction bands' [36,37].

The three types of deformation bands (dilational, isochoric, compactional) accumulate shear strain independent of frictional sliding (i.e., faulting). Coulomb frictional slip can and does occur as a *secondary* process within the tabular thickness of the bands after sufficient strain-induced changes in material strength have occurred; i.e., strain-hardening or strain-softening, depending on the mode of the pre-peak inelastic strain [25].

In summary, inelastic deformation of granular geomaterials is manifest through a variety of tabular discontinuities. Importantly, each type of discontinuity corresponds to a specific range of causative stress magnitudes. Therefore these discontinuities are useful pressure gauges of past magnitudes of the causative effective stresses. The presence of shear offsets along these discontinuities (indicating a non-trivial Q) can be determined from observations of offset bedding or other cross-cut structures in the field (e.g., [38,39]). A range of magnitudes for the causative P can be determined from the style of volumetric strain (dilation or compaction), which commonly requires microstructural observations of the discontinuity in thin section (e.g., [24,42]).

3. Approach

In this section, field and microstructural observations are used to quantify the magnitudes of stress that are required to produce observed styles of localized inelastic strain within the Wingate Sandstone at Upheaval Dome. The Wingate Sandstone is selected for this analysis because its mechanical strength is ideal for testing for the large magnitudes of stress that are associated with meteoritic impact. This analysis requires the construction of a capped strength envelope for Wingate Sandstone and the identification of the style of its inelastic strain at Upheaval Dome.

3.1. Defining the capped strength envelope

Results of laboratory testing show that a capped strength envelope for granular geomaterials can be approximated as a half-ellipse [22]:

$$\frac{\left(\frac{P}{P^*}-\delta\right)^2}{(1-\delta)^2}+\frac{\left(\frac{Q}{P^*}\right)^2}{\gamma^2}=1 \tag{3}$$

Here, Q is non-negative, P is compression positive, and δ and γ are standard unit-less coefficients that relate this empirical strength envelope to laboratory test data of rock strength. Laboratory testing of a range of granular geomaterials has shown that the δ coefficient is *ca.* 0.5, and values of γ range between 0.5 and 0.7 [22]. The critical grain crushing pressure P^* in sandstones can be determined either experimentally, or through the empirical relation

$$P^* = (\Phi R)^{-1.5} \tag{4}$$

where Φ is porosity and R is average grain radius in millimeters [30]. Therefore by using Eqs. (3) and (4), the capped strength envelope for a granular geomaterial can be calculated from measurements of porosity and grain size. Although other shape functions for the capped strength envelope are available (e.g., [33,34]), the approximation of Eq. (3) is adequate for the purpose of this paper.

Criteria for predicting the onset of inelastic strain are readily derived from Eq. (3), which describes the stress states for *incipient* inelastic strain. Therefore elastic strain can be predicted where

$$\frac{\left(\frac{P}{P^*}-\delta\right)^2}{(1-\delta)^2}+\frac{\left(\frac{Q}{P^*}\right)^2}{\gamma^2}<1 \tag{5}$$

and inelastic strain is predicted where

$$\frac{\left(\frac{P}{P^*}-\delta\right)^2}{(1-\delta)^2}+\frac{\left(\frac{Q}{P^*}\right)^2}{\gamma^2}>1 \tag{6}$$

Additionally, inelastic strain is predicted to be dilational where $P<P^*/2$, is isochoric where $P=P^*/2$ and is compactional where $P>P^*/2$ [22,24] (Fig. 5). Shear strain is predicted at all non-trivial magnitudes of Q.

Eqs. (3) and (4) show that smaller values of porosity and grain radius correspond to larger magnitudes of P^*, which in turn lead to strength envelopes that span larger magnitudes of P. This means that the style of strain in rocks with larger strength envelopes varies over a wider range and larger magnitudes of the causative mean stress, than rocks with smaller strength envelopes [22,24]. Therefore at Upheaval Dome, the large magnitudes of P that are consistent with meteoritic impact can be most readily discerned from the smaller magnitudes of stress associated with other geologic processes through analysis of the styles of strain in rocks that are fine-grained and have a low porosity.

Non-deformed Wingate Sandstone exposed at Colorado National Monument (*ca.* 100 km northwest of Upheaval Dome) has average grain radii of 0.05 mm and porosities of 20% to 24% void space by volume and contains ca. 95% quartz with sparse ferruginous cement [19,44]. These values of average grain size and porosity are smaller than other major sandstone units at Upheaval

Table 1
Parameters used to calculate the capped strength envelopes shown in Fig. 6

Fig. 6 envelope	R (mm)	Φ	P^* (GPa)	δ	γ	Source
Navajo Sandstone	0.05	0.24	0.76	0.6	0.5	[40,41]
Kayenta Formation Sandstone	0.15	0.21	0.18	0.6	0.5	[22]
Wingate Sandstone	0.05	0.20	1.00	0.6	0.5	[43,44]
White Rim Sandstone	0.141	0.19	0.23	0.6	0.5	[8]

Only the major sandstone units exposed at Upheaval Dome are listed. Φ is porosity by volume, and δ and γ are empirical curve-fitting coefficients derived by laboratory testing.

Dome (Table 1). Thus, of all the major sandstone units at Upheaval Dome, the Wingate Sandstone will exhibit inelastic deformation over the widest range of causative P (Fig. 6). Therefore the Wingate Sandstone is the best candidate for discerning the large magnitudes of impact-induced mean stress.

3.2. Microstructural analysis of non-deformed Wingate Sandstone

A series of microstructural observations of non-deformed Wingate Sandstone have been undertaken in order to define the capped strength envelope for this rock. As part of a separate study [42] samples of Wingate Sandstone were collected from erosional exposures within Cache Valley, on the road to the Island in the Sky entrance to Canyonlands National Park, approximately 30 km northeast of Upheaval Dome. Five non-deformed samples of Wingate Sandstone are collected at 0611613E 4279269N (UTM zone 12N, NAD83). The sample area is located well outside of Upheaval Dome and lacks deformation bands.

These samples of Wingate Sandstone were impregnated with a blue resin to aid in identifying void space (porosity) in thin section. Color photomicrographs of these thin sections were used to measure porosity and average grain radius of the non-deformed Wingate Sandstone. As the inter-granular space is filled with a blue resin and natural cementation is sparse, porosity is calculated for each column of pixels as the ratio of blue pixels to total pixels in that column. Fig. 7 demonstrates the results of this method for a deformed sample of Wingate Sandstone.

Our analysis of non-deformed samples of Wingate Sandstone yields porosities, Φ, of 16.9%±1.9% by volume and grain radii, R, of 0.034 mm±1.9 mm. These results are consistent with the porosities and grain radii previously reported for the Wingate Sandstone at Colorado National Monument by Lohnman [43] and Stearns and Jamison [44]. Using these values of Φ and R in Eq. (4), the corresponding magnitude of P^* is calculated to be 2.98 GPa±1.65 GPa.

Calcite staining of the thin sections reveals no evidence for calcium cementation, and pressure solution between grain contacts is not observed. Thus secondary digenetic processes have a negligible effect on the measured porosity. The presence of secondary cementation would have increased the magnitude of P^* for the host rock [24,45,46].

A set of capped strength envelopes for Wingate Sandstone are calculated using Eq. (3). Fig. 8 shows two pairs of strength envelopes calculated from the maximum and minimum values of δ, γ, and P^*, as listed in Table 2. Values for the empirical coefficients δ and γ in Eq. (3) are taken from Wong et al. [22]. The Wingate Sandstone has a larger strength envelope than other major sandstone units at Upheaval Dome (c.f., Fig. 6), as can be expected from the Wingate Sandstone's larger magnitude of $P*$.

Envelope A places a lower bound on the minimum magnitudes of Q and P that are required to produce inelastic deformation within Wingate Sandstone. Envelope D places an upper bound on the magnitudes of these stresses. Therefore analysis of envelope A is the most pertinent for the goal of this paper. Here we intend to establish the minimum range of stress magnitudes (as a conservative threshold) that are required to produce the observed style of inelastic deformation within the Wingate Sandstone at Upheaval Dome.

Natural variability in primary grain size and porosity within the Wingate Sandstone is accounted for in our

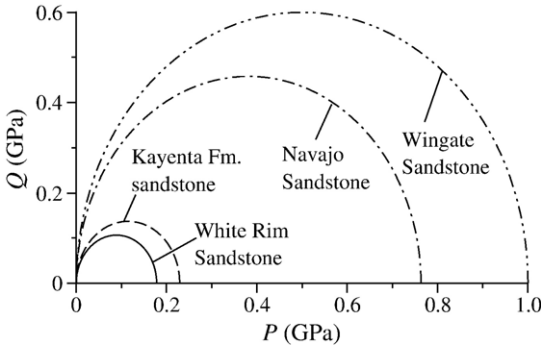

Fig. 6. Capped strength envelopes calculated using Eqs. (3) and (4) with previously reported values of average porosity (Φ) and grain radius (R) for the major sandstone units exposed at Upheaval Dome. See Table 1 for specific values and sources. The magnitudes of Φ and R influence the size of the strength envelope. The Wingate Sandstone has a relatively low porosity and small grain radius, and thus a relatively large strength envelope. The Kayenta Sandstone, on the other hand, has a relatively high porosity and large grain radius, and thus has a relatively small strength envelope.

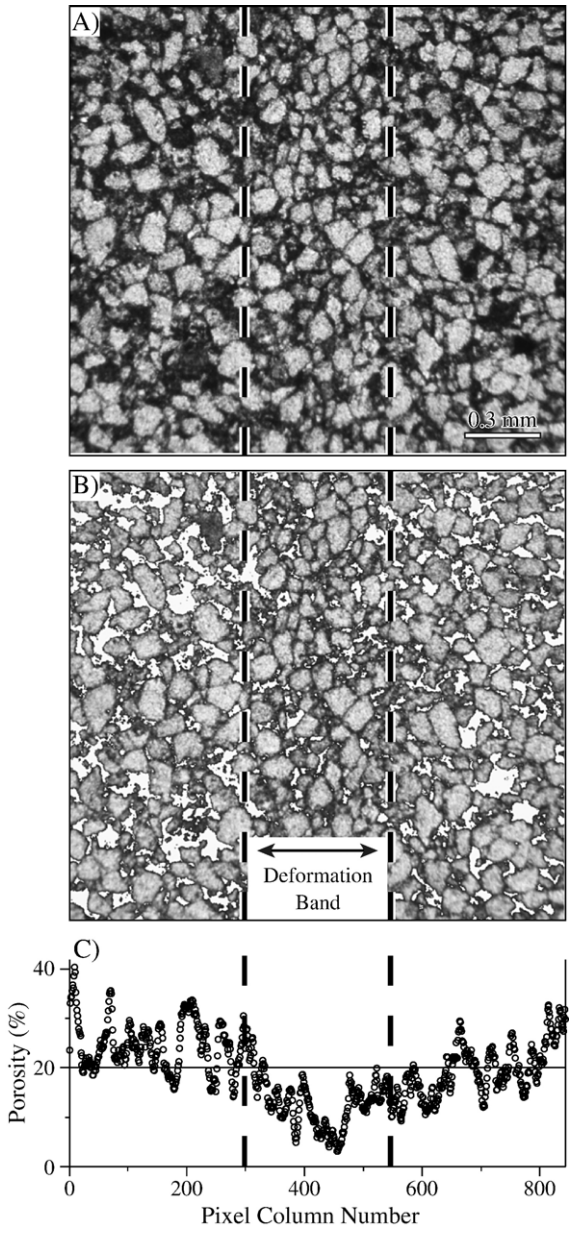

Fig. 7. (A) Photomicrograph of a deformation band in Wingate Sandstone from Upheaval Dome. The dashed vertical lines outline the band. (B) Same photomicrograph as in (A) but with the blue-resin-filled void space digitally removed to aid in visualizing the distribution of empty inter-granular voids. The band is defined by a localized decrease in inter-granular void space. (C) Porosity for each column of pixels in the photomicrograph. Porosity is calculated for each pixel column as the ratio of the pixels containing blue-resin-filled void space to the total number of pixels in that column. See Fig. 1 for location.

analyses by adopting the most conservative (smallest grain size and lowest porosity) measured values for the non-deformed samples of Wingate Sandstone (i.e., envelope A in Fig. 8). Our conservative values are still

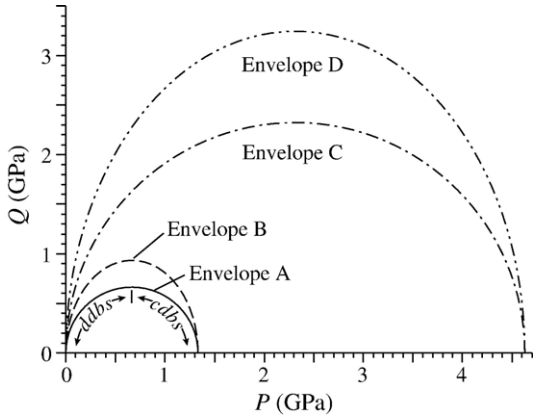

Fig. 8. Capped strength envelopes for Wingate Sandstone based on the analyses presented in this paper. Strength envelopes are calculated using minimum and maximum values of δ, γ, Φ and R. Eqs. (3) and (4) are used with the values listed in Table 2 to calculate each envelope. Envelope A places a minimum bound on the strength of the Wingate Sandstone. Dilational deformation bands (ddbs) are predicted to form at magnitudes of $P<ca.$ 0.7 GPa, while compactional deformation bands (cdbs) are predicted to form at magnitudes of $P>ca.$ 0.7 GPa.

valid lower bounds in the presence of cements since secondary cementation would act to increase rock strength (although appreciable quantities of cements are not observed in the analyzed samples).

The minimum magnitudes of causative stress for each style of localized inelastic deformation within the Wingate Sandstone can now be established based on envelope A in Fig. 8. Recall that the dilational side of the strength envelope is delineated from the compactional side by the point of isochoric shear. Isochoric shear occurs where $P=P^*/2$ and $Q=Q_{max}$. On envelope A, the point of isochoric shear corresponds to $P=0.7$ GPa and $Q=0.7$ GPa; since $\delta=\gamma$ for envelope A, the magnitude of $P^*/2$ equals the magnitude of Q_{max}. Therefore compactional inelastic deformation within the Wingate Sandstone is predicted to occur at magnitudes of P that are greater than 0.7 GPa. Dilational inelastic deformation is predicted to occur at magnitudes of P that are less than 0.7 GPa. The style of inelastic

Table 2
Parameters used to calculate the capped strength envelopes shown in Fig. 8 based on the minimum and maximum values of Φ and R calculated in this paper

Fig. 8 envelope	R (mm)	Φ	P^* (GPa)	δ	γ
A	0.04	0.19	1.33	0.5	0.5
B	0.04	0.19	1.33	0.5	0.7
C	0.02	0.15	4.63	0.5	0.5
D	0.02	0.15	4.63	0.5	0.7

deformation within the Wingate Sandstone (dilation or compaction) can now be framed in terms of causative stress magnitudes. In order to accommodate natural variability in grain size and porosity, 0.7 GPa is used through the remainder of this paper as a conservative lower bound for the transition from inelastic dilation to compaction.

3.3. Microstructural analysis of inelastic strain at Upheaval Dome

Inelastic strain in the form of cataclastic dikes [8,9] and tabular discontinuities (i.e., bands) is prevalent within the Wingate Sandstone at Upheaval Dome. The tabular discontinuities possess a component of shear, as evidenced by offset sedimentary cross-bedding (Fig. 3). The presence of shear along these bands indicates that these discontinuities are a type of deformation band for which the magnitude of the causative Q was non-trivial (c.f., Fig. 5). This paper presents analyses of the tabular discontinuities within the Wingate Sandstone as pressure gauges of past stress states.

Due to the fine-grained and low porosity character of the Wingate Sandstone, microstructural observations are required to determine whether these bands are dilational, isochoric, or compactional. In order to accomplish this analysis, samples of deformation bands within the Wingate Sandstone are collected from Upheaval Dome. Three samples are collected at 0592687E 4254482N, and one sample of deformed Wingate Sandstone is collected at 0593215E 4253971N (UTM zone 12N, NAD83). Sample locations are at radial distances of approximately 1 km from the present day center of Upheaval Dome (Fig. 1). These samples are impregnated with blue resin, and the resulting thin sections are stained to identify calcite cementation within the bands. Porosity is then calculated from photomicrographs using the same image analysis method as for the non-deformed samples (Fig. 7).

4. Results

Microstructural observations of the sampled deformation bands reveal the diagnostic characteristics of inelastic compaction. Porosity measurements indicate a decrease in deformation band porosity relative to the surrounding sandstone (Fig. 7). Porosity within the band is calculated as 5.8%±2.7% by volume from 5 deformation band samples. These porosities are significantly less than the average porosities of the non-deformed reference samples of Wingate Sandstone, which are 16.9%±1.9% by volume.

The observed reduction in porosity for the deformed samples of Wingate Sandstone parallels similar porosity reductions observed in deformed samples of White Rim Sandstone at Upheaval Dome. Kenkmann [8] reports a porosity of 19% for non-deformed White Rim Sandstone and >2% porosity for deformed samples from within clastic dikes. This reduction in porosity is attributed to grain crushing and filling of void space with comminuted material. Microstructural observations reveal no additional evidence of porosity loss due to band-filling cements or pressure solution between grain contacts. Therefore the measured decrease in deformation band porosity is attributed to the reduction of inter-granular space due to band formation rather than secondary digenetic processes.

The deformation bands also exhibit grain processing that is indicative of inelastic compaction (Fig. 9). Occasional grain crushing is observed within the bands. Grain packing geometries with greater packing efficiency (less inter-granular space) relative to the non-deformed rock are also observed within the bands.

The measured decrease in deformation band porosity due to the collapse of inter-granular space and the observations of grain crushing and increased packing efficiency are clear lines of evidence for compactional inelastic strain along the bands. Macroscopic observations of offsets of original sedimentary layering along

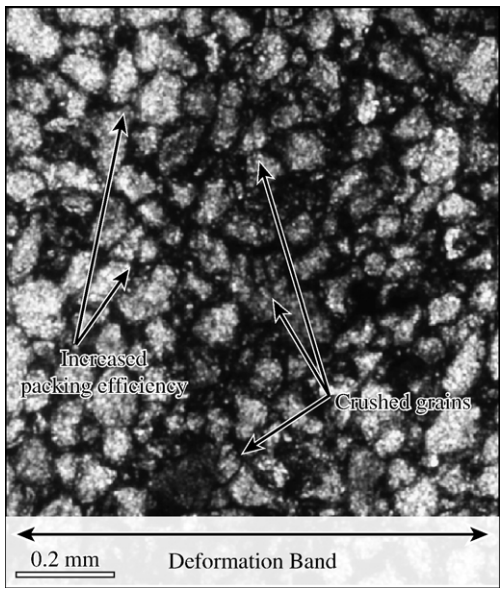

Fig. 9. Photomicrograph of the interior of a deformation band within Wingate Sandstone from Upheaval Dome. The constituent grains show evidence of increased packing efficiency and grain crushing (c.f., Fig. 4). These observations indicate that the band has accommodated compactional inelastic strain. Thus this is a compactional deformation band.

the bands show that these bands have also accommodated inelastic shear strain. These independent sets of observations unambiguously document the occurrence of compactional deformation bands within the Wingate Sandstone at Upheaval Dome. This means that the Wingate Sandstone at Upheaval Dome was subjected to at least, and possibly greater than, 0.7 GPa of mean stress (P), with a non-trivial magnitude of Q.

5. Discussion

Our analysis has shown that a minimum magnitude of P of 0.7 GPa is required to nucleate the observed compactional deformation bands within the Wingate Sandstone. This result is consistent with previous findings of GPa-scale mean stresses within the central uplift of Upheaval Dome (c.f., [4,6,8,9]). Thus evidence for GPa-scale mean stresses at Upheaval Dome is now documented from within the Wingate Sandstone, adding to previously documented results from the stratigraphically older Moenkopi Formation and White Rim Sandstone from within the central uplift.

We can now test the various geologic processes that may have plausibly occurred in the region of Upheaval Dome in order to identify specific processes that could have led to the formation of the observed compactional deformation bands within the Wingate Sandstone.

We first test the possibility that the compactional deformation bands within the Wingate Sandstone formed through tectonic processes. To do this, we assume an Andersonian stress state for faulting, with the effective lithostatic load acting as a causative principal stress. In this stress state, the magnitude of P is the mean of the effective minimum (σ_h') and maximum (σ_H') horizontal principal stresses and the effective lithostatic load (σ_V'). The magnitude of maximum differential stress (i.e., Q) is the difference between the maximum and minimum principal stress.

The maximum value of P that can be attained by this 'tectonic' system of principal stresses is limited by the largest magnitude of lithostatic load that could have acted on the Wingate Sandstone. This maximum value of lithostatic load is calculated from the maximum depth of burial for the Wingate Sandstone at Upheaval Dome. Regional exposures suggest a maximum depth of burial for the Wingate Sandstone of 2.2 km, during the Tertiary period [13]. Assuming an average overburden density of 2450 kg/m^3 (e.g., [42,47]), this depth of burial corresponds to a maximum of *ca.* 52 MPa of lithostatic load (σ_V') acting on the Wingate Sandstone under dry groundwater conditions and a maximum of *ca.* 30 MPa of lithostatic load under fully saturated groundwater conditions. The magnitude of lithostatic load for dry groundwater conditions is assumed in the following analyses. This serves as an upper limit on the maximum admissible value of σ_V' that could have acted on the Wingate Sandstone.

The maximum value of P (and attendant Q) for this tectonic loading scenario is calculated by finding the maximum magnitudes of σ_h' and σ_H', with σ_V' equal to 52 MPa, that satisfies Eq. (3). Larger magnitudes of principal stress are required to form compactional deformation bands than are required to form dilational deformation bands (Figs. 5, 8). Thus the causative stress state is chosen so as to maximize the magnitudes of the horizontal principal stresses (σ_h' and σ_H') while maintaining the vertical principal stress equal to lithostatic load (σ_V'). To minimize Q and thereby maximize the potential magnitude of P, σ_h' and σ_H' are set equal and σ_V' is assumed to be the minimum principal stress. This is the Andersonian stress state for thrust faulting.

In the assumed Andersonian stress state for thrust faulting, $\sigma_1=\sigma_h'=\sigma_H'$ and $\sigma_3=\sigma_V'=52$ MPa. Eqs. (1) and (2) relate this system of principal stresses to magnitudes of Q and P as

$$Q = \sigma_H' - \sigma_V' \tag{7}$$

$$P = \frac{2\sigma_H' - \sigma_V'}{3} \tag{8}$$

The magnitude of P^* for non-deformed Wingate Sandstone was previously calculated as 2.98 GPa± 1.65 GPa. For this analysis, P^* is assumed to be 1.33 GPa as a conservative lower limit. The maximum value of σ_H that can satisfy Eq. (3) is found to be 0.54 GPa, assuming $\delta=0.5$ and $\gamma=0.5$. Magnitudes of σ_H that are greater than 0.54 GPa will induce inelastic strain within the Wingate Sandstone at the assumed depth (i.e., satisfy Eq. (4)). These magnitudes of σ_H and σ_V correspond to a value for P of *ca.* 0.2 GPa. This means that a tectonically driven P could not be any larger than *ca.* 0.2 GPa before deformation bands begin to form within the Wingate Sandstone.

An Andersonian stress state for thrust faulting provides an upper limit to the maximum magnitude of P that can be achieved before inelastic strain occurs within the Wingate Sandstone under tectonic loading conditions. The maximum magnitude of P from an Andersonian stress state for normal faulting is much smaller. Assuming that $\sigma_3=\sigma_h'=\sigma_H'$ and $\sigma_1=\sigma_V'=$ 52 MPa (i.e., a stress state for normal faulting) and $\delta=0.5$, $\gamma=0.5$ and $P^*=1.33$ GPa, the value for P in a

normal fault stress state is found to be *ca.* 0.05 GPa. Therefore the thrust fault stress state places an upper limit on the maximum magnitude of P that can be feasibly attained under tectonic loading conditions.

Accordingly we find that under tectonic loading conditions, P could not be any larger than *ca.* 0.2 GPa before deformation bands begin to form within the Wingate Sandstone at Upheaval Dome. Because this value of P is much less than $P^*/2$ for the Wingate Sandstone (0.7 GPa), any resulting inelastic (tectonic) strain is predicted to be manifested as dilational deformation bands. The magnitude of P cannot become sufficiently large (with lithostatic load as the principal stress) to nucleate compactional deformation bands under tectonic loading conditions.

This analysis shows that compactional deformation bands are not predicted to nucleate within the Wingate Sandstone at Upheaval Dome when lithostatic load alone acts as a causative principal stress. The observed compactional deformation bands at Upheaval Dome are not adjacent to through-going faults, and thus fault-induced static stress changes (e.g., [42]) do not readily explain their occurrence either. In diapiric processes, the vertical component of the stress state is generally controlled by lithostatic load (similar to the tectonic loading scenario). Thus salt diapirism, or dissolution (e.g., [48]), does not readily explain the formation of the observed compactional deformation bands because lithostatic load, as σ_V, is again the major component of a causative principal stress. This line of reasoning also excludes plutonic intrusion as a viable process for forming these bands.

Through our analyses of potential causative stress states, we can now rule out static tectonic stress change, plutonic intrusion, and salt diapirism as causes for the observed compactional deformation bands within the Wingate Sandstone at Upheaval Dome. These processes are limited by the maximum plausible magnitude of lithostatic load, given the regional geologic history and structure. These processes cannot generate sufficient magnitudes of P to cause the nucleation of the observed compactional deformation bands within the Wingate Sandstone at Upheaval Dome.

The magnitudes of P revealed through our analyses are consistent with the magnitudes of stress that have been previously attributed to meteoritic impact processes at Upheaval Dome ([4,6,8,9] and others). The range of P over which the observed compactional deformation bands will form within the Wingate Sandstone (*ca.* 0.7 GPa to 1.4 GPa) is consistent with the magnitudes of causative mean stress interpreted for the planar-deformed quartz in the White Rim Sandstone (*ca.* 0.25 GPa to 3.0 GPa; [6,8,9]). Thus deformation in the White Rim Sandstone and Wingate Sandstone may well have been contemporaneous. Furthermore, numerical model simulations of an impact origin for Upheaval Dome by Kenkmann et al. [9] predict approximately 1 GPa to 4 GPa of maximum mean stress within the Wingate Sandstone during the shock compression stage of crater growth [49] at the radial distance where the present study's deformed samples were collected. Thus a meteoritic impact is predicted to have generated a sufficient magnitude of mean stress to induce the formation of the observed compactional deformation bands.

Therefore we find that the observed compactional deformation bands within the Wingate Sandstone formed by, and are additional evidence of, a meteoritic impact at Upheaval Dome. The presence of impact-related deformation within the Wingate Sandstone places the impact event after the formation of the Wingate Sandstone, which was deposited during the Early Jurassic.

6. Implications

Upheaval Dome is an ideal location to study processes related to meteoritic impacts, including: the mechanics of cratering within sedimentary rock, the effects of cratering on the micro- and macrostructure of the target materials, and the relationship between geophysical 'damage zones' around craters (e.g., [50]) and manifestations of inelastic deformation observed in the field. The extensive exposures available at Upheaval Dome may be especially helpful in understanding the effects of dynamic strength degradation during impact (e.g., [49,51–53]) into granular rocks and soils and the resulting styles of inelastic deformation.

Small 'faults' that are seemingly analogous to the deformation bands studied in this paper have been reported elsewhere at Upheaval Dome within sandstone units of the Chinle and Kayenta Formations [9] and within cataclastic dikes of White Rim Sandstone [8]. Morphologically comparable 'microbreccia' zones have also been reported at other impact craters [54]. The approach documented in this paper can be applied to these features to yield additional insight into the distribution of stresses during impact.

The compactional deformation bands discussed here show no evidence of pseudotachylite (friction melt; [55]) formation in thin section. Indeed, pseudotachylites have not been reported at Upheaval Dome. Pseudotachylite can be expected to form along a 1 mm think shear zone that is longer than 3 cm to 30 cm and has a

shear strain of 3% to 10% [56]. The compactional deformation bands within the Wingate are typically several tens of centimeters in length and 1 mm to 3 mm in width. The magnitude of maximum shear strain along these bands is unconstrained by the present study, but is typically <0.5% for deformation bands that lack slip surfaces in other sandstones (e.g., [39,57]). Thus the lack of pseudotachylite along the compactional deformation bands discussed here can be attributed to the magnitude of shear strain, and possibly strain rate and applied stresses, being insufficient for pseudotachylite formation. Future work in this area may help to place an upper limit on the magnitudes of stresses that were present when these deformation bands formed.

Compactional deformation bands in general are not unique to impact craters. Many examples of fault-related compactional deformation bands exist (e.g., [21–26]). Therefore application of our approach to other impact craters requires geomechanical analyses such as those presented in this paper in order to establish a link between any observed compactional deformation bands and impact processes. This approach may be especially useful at deeply eroded impact craters in sedimentary rock, where evidence of high velocity impact (e.g., planar-deformed quartz, shatter cones, etc.) is not observed.

7. Conclusion

Tabular discontinuities observed within the Wingate Sandstone at Upheaval Dome accommodate localized shear displacements, compaction of inter-granular space, grain crushing, and increased grain packing efficiency relative to the non-deformed host rock. These discontinuities are therefore identified as compactional deformation bands. The capped strength envelope for Wingate Sandstone reveals that compactional deformation bands require between 0.7 GPa and 4.6 GPa of mean stress (P) in order to nucleate. These magnitudes of mean stress are consistent with numerical model predictions of a meteoritic impact at Upheaval Dome. The magnitudes of mean stress that can be generated by diapirism and static tectonic stress change at Upheaval Dome are insufficient to drive the growth of compactional deformation bands within the Wingate Sandstone. Therefore these deformation bands are additional evidence of an impact event at Upheaval Dome. This finding also supports a post-Wingate (post-Early Jurassic) age for this impact.

Acknowledgements

We are grateful for comments from Christian Koeberl and an anonymous reviewer, which improved the clarity and scope of this manuscript. We thank Charles Schelz and Vicki Webster for expediting research permits within Canyonlands National Park. Thanks also to Roger Soliva and P. Eeps for help in obtaining samples of Wingate Sandstone.

References

[1] P. Huntoon, G. Billingsley, W. Breed, Geologic Map of Canyonlands National Park and vicinity, Utah, Canyonlands Nat. Hist. Assoc., Moab, UT, 1982.
[2] U.S. Geological Survey, Upheaval Dome Digital Orthophoto Quadrangle, 1993.
[3] P. Huntoon, Upheaval Dome, Canyonlands, Utah: strain indicators that reveal an impact origin, in: D.A. Sprinkel, T.C. Chidsey Jr., P.B. Anderson (Eds.), Geology of Utah's Parks and Monuments, Publication, vol. 28, Utah Geological Association, 2000, pp. 1–10.
[4] E. Shoemaker, K. Herkenhoff, Upheaval Dome impact structure, Lunar Planet. Sci. Conf. Houston 15 (1984) 778–779.
[5] P. Huntoon, E. Shoemaker, Roberts Rift, Canyonlands, Utah: a natural hydraulic fracture caused by comet or asteroid impact, Ground Water 3 (1995) 561–569.
[6] B. Kriens, E. Shoemaker, K. Herkenhoff, Geology of the Upheaval Dome impact structure, southeast Utah, J. Geophys. Res. 104 (1999) 18867–18887.
[7] Z. Kanbur, J. Louie, S. Chávez-Pérez, G. Plank, D. Morey, Seismic reflection study of Upheaval Dome, Canyonlands National Park, Utah, J. Geophys. Res. 105 (2000) doi:10.1029/1999JE001131.
[8] T. Kenkmann, Dike formation, cataclastic flow, and rock fluidization during impact cratering: an example from the Upheaval Dome structure, Utah, Earth Planet. Sci. Lett. 214 (2003) 43–58.
[9] T. Kenkmann, A. Jahn, D. Scherler, B. Ivanov, Structure and formation of a central uplift: a case study at Upheaval Dome impact crater, Utah, in: T. Kenkmann, T. Hörz, A. Deutsch (Eds.), Large Meteorite Impacts III, Geol. Soc. Am. Paper, vol. 384, 2005, pp. 85–115.
[10] E. McKnight, Geology of area between Green and Colorado Rivers, Grand and San Juan Counties, Utah, U.S. Geol. Surv. Bull. 908 (1940) (147 pp).
[11] H. Joesting, D. Plouff, Geophysical studies of the Upheaval Dome area, San Juan County, Utah, 9th Annual Field Conference Guidebook, Intermountain Association of Petroleum Geologists, 1958, pp. 86–92.
[12] R. Mattox, Upheaval Dome, a possible salt dome in the Paradox basin, Utah, in: R.B. Mattox (Ed.), Saline Deposits, Geol. Soc. Am. Spec. Paper, vol. 88, 1968, pp. 331–347.
[13] M. Jackson, D. Schultz-Ela, M. Hudec, I. Watson, M. Porter, Structure and evolution of Upheaval Dome, a pinched-off salt diapir, Geol. Soc. Amer. Bull. 110 (1998) 1547–1573.
[14] W. Bucher, Cryptovolcanic structures in the United States, Report of the 16th Session (1933), International Geological Congress, Washington, DC, 1936, pp. 1055–1084.
[15] R. Kopf, Hydrotectonics, principles and relevance, U.S. Geol. Surv. Open-File Report, 1982, pp. 82–307, 13 pp.
[16] T. Kenkmann, Folding within seconds, Geology 30 (2002) 231–234.
[17] D. Baratoux, H.J. Melosh, The formation of shatter cones by shock wave interference during impacting, Earth Planet. Sci. Lett. 216 (2003) 43–54.

[18] C. Koeberl, J.B. Plescia, C.L. Hayward, W.U. Reimold, A petrographical and geochemical study of quartzose nodules, country rocks, and dike rocks from the Upheaval Dome structure, Utah, Meteorit. Planet. Sci. 34 (1999) 861–868.
[19] S.W. Kieffer, Shock metamorphism of the Coconino Sandstone at meteor Crater, Arizona, J. Geophys. Res. 76 (1971) 5449–5473.
[20] W. Alvarez, E. Staley, D. O'Connor, M. Chan, Synsedimentary deformation in the Jurassic of southeastern Utah—a case of impact shaking? Geology 26 (1998) 579–582.
[21] T.-F. Wong, H. Szeto, Z. Zhang, Effect of loading path and porosity on the failure mode of porous rocks, Appl. Mech. Rev. 45 (1994) 281–293.
[22] T.-F. Wong, C. David, W. Zhu, The transition from brittle faulting to cataclastic flow in porous sandstones: mechanical deformation, J. Geophys. Res. 102 (1997) 3009–3025.
[23] Y. Guéguen, M. Boutéca, Mechanics of Fluid-saturated Rocks, Elsevier, Amsterdam, 2004, 450 pp.
[24] T.-F. Wong, C. David, B. Menéndez, Mechanical compaction, in: Y. Guéguen, M. Boutéca (Eds.), Mechanics of Fluid-saturated Rocks, Elsevier, Amsterdam, 2004, pp. 55–114.
[25] R.A. Schultz, R. Siddharthan, A general framework for the occurrence and faulting of deformation bands in porous granular rocks, Tectonophysics 411 (2005) 1–18.
[26] A. Aydin, R.I. Borja, P. Eichhubl, Geological and mathematical framework for failure modes in granular rock, J. Struct. Geol. 28 (2006) 83–98.
[27] A. Schofield, P. Wroth, Critical State Soil Mechanics, McGraw-Hill Book Company, New York, 1968, 310 pp.
[28] J. Heyman, Coulomb's Memoir on Statics: An Essay in the History of Civil Engineering, Cambridge University Press, Cambridge, 1972, 211 pp.
[29] E. Hoek, E. Brown, Empirical strength criterion for rock masses, J. Geotech. Eng. Div. ASCE 106 (1980) 1013–1035.
[30] J. Zhang, T.-F. Wong, D.M. Davis, Micromechanics of pressure-induced grain crushing in porous rocks, J. Geophys. Res. 95 (1990) 341–352.
[31] K. Roscoe, J. Burland, On the generalized stress–strain behavior of 'wet' clay, in: J. Heyman, F. Leckie (Eds.), Engineering Plasticity, Cambridge University Press, Cambridge, 1968, pp. 535–609.
[32] K. Issen, J. Rudnicki, Conditions for compaction bands in porous rock, J. Geophys. Res. 105 (2000) 21529–21536.
[33] K. Issen, The influence of constitutive models on localization conditions for porous rock, Eng. Fract. Mech. 69 (2002) 1891–1906.
[34] R.I. Borja, A. Aydin, Computational modeling of deformation bands in granular media: I. Geological and mathematical framework, Comput. Methods Appl. Mech. Eng. 193 (2004) 2667–2698.
[35] X. Du Bernard, P. Eichhubl, A. Aydin, Dilation bands: a new form of localized failure in granular media, Geophys. Res. Lett. 29 (2002) doi:10.1029/2002GL015966.
[36] P. Mollema, M. Antonellini, Compaction bands: a structural analog for anti-mode I cracks in aeolian sandstone, Tectonophysics 267 (1996) 209–228.
[37] T.-F. Wong, P. Baud, E. Klein, Localized failure modes in compactant porous rock, Geophys. Res. Lett. 28 (2001) 2521–2524.
[38] A. Aydin, Z. Reches, Number and orientation of fault sets in the field and in experiments, Geology 10 (1982) 107–112.
[39] H. Fossen, J. Hesthammer, Geometric analysis and scaling relations of deformation bands in porous sandstone, J. Struct. Geol. 19 (1997) 1479–1493.
[40] A. Aydin, Small faults formed as deformation bands in sandstones, Pure Appl. Geophys. 116 (1978) 913–930.
[41] W.L. Stokes, Geology of Utah, Utah Mus. of Nat. Hist. and Utah Geol. and Miner. Surv., Salt Lake City, 1986, 280 pp.
[42] C.H. Okubo, R.A. Schultz, Evolution of damage zone geometry and intensity in porous sandstone: insight gained from strain energy density, J. Geol. Soc. (Lond.) 162 (2005) 939–949.
[43] S.W. Lohnman, Geology and artesian water supply of the Grand Junction area, Colorado, U.S. Geol. Surv. Professional Paper, vol. 451, 1965, 149 pp.
[44] D. Stearns, W. Jamison, Deformation of sandstones over basement uplifts, Colorado National Monument, in: H. Veal (Ed.), Exploration Frontiers of the Central and Southern Rockies, Rocky Mountain Association of Geologists, 1977, pp. 31–39.
[45] B. Menéndez, W. Zhu, T.-F. Wong, Micromechanics of brittle faulting and cataclastic flow in Brea Sandstone, J. Struct. Geol. 18 (1996) 1–16.
[46] C. David, B. Menéndez, Y. Bernabé, The mechanical behavior of synthetic sandstone with varying brittle cement content, Int. J. Rock Mech. Min. Sci. 35 (1998) 759–770.
[47] R.D. Lama, V.S. Vutukuri, Handbook on Mechanical Properties of Rocks, Testing Techniques and Results, vol. II, Trans Tech Publications, Clausthal, Germany, 1978, 481 pp.
[48] H. Ge, M.P.A. Jackson, Physical modeling of structures formed by salt withdrawal: implications for deformation caused by salt dissolution, AAPG Bull. 82 (1998) 228–250.
[49] H.J. Melosh, B.A. Ivanov, Impact crater collapse, Annu. Rev. Earth Planet. Sci. 27 (1999) 385–415.
[50] K. Xia, T.J. Ahrens, Impact induced damage beneath craters, Geophys. Res. Lett. 28 (2001) 3525–3527.
[51] H.J. Melosh, E.S. Gaffney, Acoustic fluidization and the scale dependence of impact crater morphology, J. Geophys. Res. 88 (1983) A830–A834.
[52] H.J. Melosh, Dynamical weakening of faults by acoustic fluidization, Nature 379 (1996) 601–606.
[53] K. Wüennemann, B.A. Ivanov, Numerical modeling of the impact crater depth-diameter dependence in an acoustically fluidized target, Planet. Space Sci. 51 (2003) 831–845.
[54] I.P. Sweet, P.W. Haines, K. Mitchell, Matt Wilson structure: record of an impact event of possible Early Mesoproterozoic age, Northern Territory, Aust. J. Earth Sci. 52 (2005) 675–688.
[55] W.U. Reimold, R.L. Gibson, "Pseudotachylites" in large impact structures, in: C. Koeberl, H. Henkel (Eds.), Impact Tectonics, Springer, Berlin, 2005, pp. 1–53.
[56] H.J. Melosh, The mechanics of pseudotachylite formation in impact events, in: C. Koeberl, H. Henkel (Eds.), Impact Tectonics, Springer, Berlin, 2005, pp. 55–80.
[57] R.A. Schultz, H. Fossen, Displacement-length scaling in three dimensions: the importance of aspect ratio and application to deformation bands, J. Struct. Geol. 24 (2002) 1389–1411.